Stability properties of a resonant cascade laser

G. J. de Valcárcel
Departament de Física Aplicada, Universitat Politècnica de Valencia, Escuela Técnica Superior de Ingenieros Industriales, 46071-Valencia, Spain

Eugenio Roldán
Departament d'Optica, Universitat de València, 46100-Burjassot, Spain

R. Vilaseca
Departament de Física i Enginyeria Nuclear, Universitat Politècnica de Catalunya, 08222-Terrassa, Spain
(Received 23 June 1993)

The emission of a resonant nondegenerate cascade laser in which up to two fields can be simultaneously amplified inside a cavity is theoretically investigated. Each field is resonantly coupled with one of the transitions of a ladder three-level atomic system, in conditions of homogeneous broadening. General analytical expressions for zero-, one-, and two-field solutions are given. Cooperative emission between both fields is found. Through the linear stability analysis of these solutions we obtain phase diagrams showing their respective domains of stability. Together with the existence of Hopf bifurcations associated with one-photon processes, which coincide with those of a Lorenz-Haken laser, a genuine Hopf bifurcation due to two-photon processes has been found. This last bifurcation does not require the "bad cavity" nor the "Lorenz threshold" conditions. The stability of the orbits that bifurcate from these critical points is analytically investigated. For this we have rewritten one of the standard criteria in a useful and straightforward way. Finally, the dynamic regimes exhibited by the system well above the instability thresholds is numerically investigated revealing transitions to chaos via quasiperiodicity.

PACS number(s): 42.55.−f, 42.60.Mi, 47.20.Ky, 05.45.+b

I. INTRODUCTION

The theoretical and experimental investigations on laser dynamics have mostly concentrated on single-mode lasers and on multimode lasers in which all the modes are coupled to a unique transition of the atoms or molecules constituting the amplifying medium [1]. In the present work we study the dynamics of a new class of bimode (or bichromatic) laser in which the two fields that can be amplified inside the cavity are coupled to two different transitions of the amplifying medium. These two transitions share a common level, so that three atomic or molecular levels defining a cascade (or ladder) scheme are involved. In this radiation-matter interaction configuration new mode competition or cooperation phenomena appear, which are brought about by the sharing of the intermediate-level population and by the presence of two-photon processes connecting the upper and lower levels. These new phenomena participate in the radiation amplification process and, consequently, the steady state and the dynamic behavior of this class of laser should be richer than those observed in most other laser classes investigated so far.

When the two amplified fields are resonant or quasiresonant with their respective transitions, the system is properly called a cascade laser. In contrast, in the limit of a large enough intermediate-level detuning the system can become a two-photon laser, if the dominant amplifying transition is the two-photon one.

The cascade lasers attracted early interest from both the experimental and theoretical points of view (see Ref. [2] and references therein). Examples of lasers operating on cascade transitions are the efficient CO laser and the He-Cd laser [3]. Some specific experiments on cascade lasers in other atomic or molecular media have been carried out in the past [4]. However, to our knowledge there is not any characterization of the dynamic behavior of these lasers. From the theoretical point of view effort has been devoted to the quantum description of the cascade laser [5] and in our recent paper [6] the dynamics of this laser have been partially studied. In the related case of the two-photon laser a remarkable achievement has been attained recently with the first clear operation of such a class of laser in a Ba atomic-beam medium [7]. Previous attempts were performed with He-Ne [4(a)] and Li (two-photon amplifier) [8]. In the microwave region a two-photon Rb micromaser was developed a few years ago [9]. From the theoretical point of view the main effort has also been devoted to the quantum description of the two-photon laser or maser [5,10]; the dynamics has been considered only in [11] (two-photon maser) and [12] (two-photon laser), although in this latter case a two-level model has been adopted which does not contain the cascade limit.

In the present work we theoretically investigate in detail the stability properties of a cascade laser in conditions of exact resonance of each field with its corresponding atomic (or molecular) transition. Our analysis is quite general in the sense that a broad region in the parameter space is considered (independent cavity losses and gain parameters for each field, and different relaxation rates for the population inversions, dipoles, and two-photon

coherence are allowed) in most parts of the study. This represents a considerable enlargement of our previous paper [6], in which the general model for a cascade laser was presented, and its dynamical properties were discussed in a very symmetrical case. As is described in the following sections, the present extended study has showed the existence of just two basic (and independent) kinds of Hopf bifurcations which are shared by both the single-mode and the bimode solutions. It has also evidenced that these stationary solutions are connected by pitchfork bifurcations, and that no situation of bistability or multistability exists. All these pitchfork and Hopf bifurcations have been determined by means of a linear stability analysis of the corresponding stationary solutions. The subcritical or supercritical character of the bifurcating solutions which emerge from these critical points has also been theoretically studied. Finally, the different classes of dynamic behavior as well as the roads to chaos appearing in this cascade laser model above the instability threshold have been numerically determined and characterized.

In Sec. II the cascade laser model is recalled and the notation and operating conditions are defined. In Sec. III the different possible stationary solutions are analytically obtained. In Sec. IV the linear stability analysis of each one of these solutions is carried out. In Sec. V particular illustrative cases are considered for which phase diagrams showing the different possible emission regimes are obtained. The stability of the periodic orbits which emerge from the Hopf bifurcation points is also determined through nonlinear analysis (the details are given in the Appendix). In Sec. VI the different dynamics of the system associated with local bifurcations and large-size attractors are presented in appropriate phase diagrams. The characterization of the different periodic, quasiperiodic, and chaotic regimes is carried out by means of time traces, attractor projections, and Poincaré sections. Finally, in Sec. VII the main conclusions are summarized and an outlook is given.

II. MODEL

As in Ref. [6], we consider a three-level active medium (levels, 1, 0, and 2) interacting with two generated electric fields $\mathcal{E}_1$ and $\mathcal{E}_2$ inside a ring cavity. The frequencies of the dipolar transitions ω_{20} and ω_{01} are assumed to be different enough, as well as the optical frequencies of the two fields, to have each field interacting with only one transition (nondegenerate case, Fig. 1).

The general equations which describe the above model are given in Ref. [6] for arbitrary values of cavity detunings and density-matrix element relaxation rates. Throughout this paper we will restrict ourselves to the case of exact resonance for each field and, for the sake of simplicity, equal relaxation rate for the two medium polarizations associated with the upper and lower transitions. This case is described by the following set of real equations:

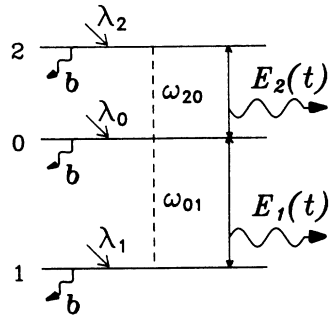

FIG. 1. Three-level system describing the amplifying medium of the cascade laser. The field E_1 (E_2) is resonantly coupled with the atom transition 0-1 (2-0). The three levels are assumed to have the same normalized external population relaxation rate b.

$$
\begin{aligned}
\dot{d}_2 &= -\gamma_{\parallel} d_2 + \lambda_2 - 4\alpha_2 y_2 + 2\alpha_1 y_1 \ , \\
\dot{y}_2 &= -\gamma_{\perp} y_2 + \alpha_2 d_2 + \alpha_1 x \ , \\
\dot{\alpha}_2 &= -\kappa_2 \alpha_2 + g_2 y_2 \ , \\
\dot{d}_1 &= -\gamma_{\parallel} d_1 + \lambda_1 - 4\alpha_1 y_1 + 2\alpha_2 y_2 \ , \\
\dot{y}_1 &= -\gamma_{\perp} y_1 + \alpha_1 d_1 - \alpha_2 x \ , \\
\dot{\alpha}_1 &= -\kappa_1 \alpha_1 + g_1 y_1 \ , \\
\dot{x} &= -\gamma x + \alpha_1 y_1 - \alpha_1 y_2 \ ,
\end{aligned}
\tag{1}
$$

where d_2 (d_1) denotes the population inversion for the upper (lower) transition, λ_i is the constant incoherent pumping rate for the inversion d_i, $y_{2\,(1)} = \mathrm{Im}[\rho_{02\,(10)}]$ is proportional to the medium polarization at the frequency of the upper (lower) transition (being ρ_{ij} the slowly varying complex amplitude of the coherence associated with transition $i-j$), α_2 (α_1) is half the Rabi frequency of the field $\mathcal{E}_2$ ($\mathcal{E}_1$), and $x = \mathrm{Re}[\rho_{12}]$ is responsible for the coherent two-photon processes through the equations of evolution for y_2 and y_1. The parameters $\gamma_{\parallel}$, $\gamma_{\perp}$, γ, and κ_i represent the damping rates for the inversions, dipoles, two-photon coherence, and the field amplitude α_i, respectively. Population decay has been assumed to occur from each level 1, 0, or 2 to other levels not included in the three-level system (external relaxation). The radiation-matter coupling constant—or gain factor—associated with the field $\mathcal{E}_i$ is

$$
g_i = \frac{N \omega_i \mu_{0i}^2}{2\epsilon_0 \hbar} \ , \tag{2}
$$

where ω_i is the reference frequency for this field, which is chosen to be that of the corresponding transition since resonance is imposed; N is the number of active molecules per unit volume; μ_{0i}^2 is the square of the modulus of the electric dipole matrix element between states $|0\rangle$ and $|i\rangle$, and ϵ_0 is the vacuum permittivity. Finally, the dots in (1) denote derivative with respect to time.

Note that Eqs. (1) are symmetric under a change of subscripts ($1 \rightarrow 2$) and the change $x \rightarrow -x$.

For the sake of clarity, and in order to deal with more

convenient control parameters for this cascade laser model, we define the following new set of variables:

$$E_i=\alpha_i/\gamma_\perp\ ,$$
$$P_i=(g_i/\kappa_i)y_i\ ,$$
$$D_i=(g_i/\kappa_i)d_i\ , \tag{3a}$$
$$Q=\sqrt{(g_1/\kappa_1)(g_2/\kappa_2)}x\ ,$$

and parameters

$$\sigma_i=\kappa_i/\gamma_\perp\ ,\quad \Gamma=\gamma/\gamma_\perp\ ,\quad b=\gamma_\parallel/\gamma_\perp\ ,$$
$$r_i=\frac{\lambda_i g_i}{\gamma_\parallel\kappa_i}\ ,\quad \chi=\frac{g_1/\sigma_1}{g_2/\sigma_2}=\frac{\omega_1}{\omega_2}\left[\frac{\mu_{10}}{\mu_{02}}\right]^2\frac{\sigma_2}{\sigma_1}\ , \tag{3b}$$

$i=1,2$, for which Eqs. (1) become

$$\dot{D}_2=b(r_2-D_2)-4E_2P_2+\frac{2}{\chi}E_1P_1\ , \tag{4a}$$
$$\dot{P}_2=-P_2+E_2D_2+\frac{1}{\sqrt{\chi}}E_1Q\ , \tag{4b}$$
$$\dot{E}_2=\sigma_2(P_2-E_2)\ , \tag{4c}$$
$$\dot{D}_1=b(r_1-D_1)-4E_1P_1+2\chi E_2P_2\ , \tag{4d}$$
$$\dot{P}_1=-P_1+E_1D_1-\sqrt{\chi}E_2Q\ , \tag{4e}$$
$$\dot{E}_1=\sigma_1(P_1-E_1)\ , \tag{4f}$$
$$\dot{Q}=-\Gamma Q+\frac{1}{\sqrt{\chi}}E_2P_1-\sqrt{\chi}E_1P_2\ . \tag{4g}$$

In Eqs. (4), r_1 and r_2 represent the pump parameter for the lower and upper transitions, respectively, and are defined as in the Lorenz-Haken model [1,13]. χ is a genuine parameter of this cascade laser model. If we interpret g_i/κ_i (i.e., the gain-over-losses ratio for the field E_i) as the system's *efficiency* for amplification of the field E_i, then χ represents the *relative efficiency* of the system for the amplification of the fields E_1 and E_2. Note that χ takes into account, on the one hand, the quotients between transition probabilities (μ_{0i}^2) and transition frequencies which are parameters of the amplifying medium; on the other hand, χ contains the quotient between cavity losses, which is a resonator parameter. Note also that Eqs. (4) are now symmetric under a change ($1\rightarrow 2$), ($Q\rightarrow -Q$), and ($\chi\rightarrow 1/\chi$).

III. STATIONARY SOLUTIONS

Depending on the fields that are null, the stationary solutions of Eqs. (4) can be classified into four types: (a) both fields are null, (b) only the field E_2 is generated, (c) only the field E_1 is generated, and (d) both fields are generated. These stationary solutions will be referred to, in the following, as (0,0), (0,E_2), (E_1,0), and (E_1,E_2), respectively, and will be analyzed separately.

A. Trivial solution (0,0)

As in any class of laser a zero-intensity solution exists which adopts the form

$$E_1=E_2=P_1=P_2=Q=0\ , \tag{5a}$$
$$D_2=r_2\ , \tag{5b}$$
$$D_1=r_1\ . \tag{5c}$$

B. Stationary solution (0,E_2)

When the upper transition 2-0 has enough gain, the field E_2 is amplified and the following solution appears:

$$D_2=1\ , \tag{6a}$$
$$P_2=E_2\ , \tag{6b}$$
$$E_2=\pm\tfrac{1}{2}\sqrt{b(r_2-1)}\ , \tag{6c}$$
$$D_1=r_1+\frac{\chi}{2}(r_2-1)\ , \tag{6d}$$
$$E_1=P_1=Q=0\ . \tag{6e}$$

Note that Eqs. (6a)–(6c) are a scaled version of the stationary solution of a two-level single-mode laser (Lorenz-Haken model [1,13]) as expected because of the existence of only one field. This type of solution will only exist if $r_2>1$, as is obvious from Eq. (6c).

C. Stationary solution (E_1,0)

In this case, at least the lower transition 0-1 has enough gain for amplification. The solution reads

$$D_2=r_2+\frac{1}{2\chi}(r_1-1)\ , \tag{7a}$$
$$E_2=P_2=Q=0\ , \tag{7b}$$
$$D_1=1\ , \tag{7c}$$
$$P_1=E_1\ , \tag{7d}$$
$$E_1=\pm\tfrac{1}{2}\sqrt{b(r_1-1)}\ . \tag{7e}$$

As in the previous case, Eqs. (7c)–(7e) are a scaled version of the Lorenz-Haken stationary solution and, analogously, it exists only if $r_1>1$.

D. Stationary solution (E_1,E_2)

When both fields are amplified, the corresponding stationary solution reads

$$D_2=1+\frac{\chi-1}{\Gamma\chi}E_1^2\ , \tag{8a}$$
$$P_2=E_2\ , \tag{8b}$$
$$E_2^2=K\left\{4\Gamma(r_2-1)+\left[\frac{1}{\chi}(b+2\Gamma)-b\right](r_1-1)\right\}\ , \tag{8c}$$
$$D_1=1+\frac{1-\chi}{\Gamma}E_2^2\ , \tag{8d}$$
$$P_1=E_1\ , \tag{8e}$$
$$E_1^2=K\left\{4\Gamma(r_1-1)+\left[\chi(b+2\Gamma)-b\right](r_2-1)\right\}\ , \tag{8f}$$

$$Q=\frac{1-\chi}{\Gamma\sqrt{\chi}}E_1E_2 , \tag{8g}$$

being

$$K=\frac{b\Gamma\chi}{b(b+2\Gamma)(\chi-1)^2+12\Gamma^2\chi} . \tag{8h}$$

Equations (8) show that the field intensities E_1^2 and E_2^2 have a linear dependence with respect to the pump parameters r_1 and r_2. Increasing the pump r_1 (r_2) causes E_1 (E_2) to grow, while E_2 (E_1) grows or decreases depending on the sign of the square brackets in Eqs. (8). In particular, only if $b/(b+2\Gamma)<\chi<(b+2\Gamma)/b$ do the two pump mechanisms cooperate, i.e., increasing r_1 or r_2 causes both field intensities to grow. These limitations in the value of χ for cooperation disappear in the case $\Gamma\to\infty$, which, according to Eq. (8g), corresponds to the absence of two-photon processes ($Q=0$). This suggests that the cooperativity between pump mechanisms comes from the step-by-step processes 2-0-1 (which obviously contribute to amplification of both fields), while the interference between them and the coherent two-photon processes can be (when destructive) responsible for the noncooperation.

Another clear example of strong cooperation is the case $\chi=1$ (equal efficiency for amplification of both fields). In this case both population inversions become equal to 1, for any value of the pump parameters, and according to Eq. (8g) $Q=0$, denoting an absence of two-photon processes in average. These two features also occur in the single-mode solutions [Eqs. (6) and (7)]. This suggests that for $\chi=1$ the presence of the field E_2 should not affect the amplification of the field E_1, and vice versa. However, this is not the case since, interestingly enough, the field intensities E_1^2 and E_2^2 reach larger values than in the single-mode cases (for instance, for $r_1=r_2=r$ one has $E_1^2=E_2^2=2E^2$, where E^2 is the single-mode intensity for the pump r). Thus cascade lasers can exhibit *cooperation* between modes through step-by-step processes.

Let us analyze next the conditions for the existence of the two-mode (or two-field) stationary solution of Eqs. (8). For the sake of later convenience, we write Eqs. (8c) and (8f) as

$$E_2^2=B_2e_3 , \tag{9a}$$

$$E_1^2=B_1c_3 , \tag{9b}$$

where $B_i=-4K/\sigma_i$ ($i=1,2$), which is always negative and

$$e_3\equiv-\frac{\sigma_2}{4}\left\{4\Gamma(r_2-1)+\left[\frac{1}{\chi}(b+2\Gamma)-b\right](r_1-1)\right\} , \tag{10a}$$

$$c_3\equiv-\frac{\sigma_1}{4}\left\{4\Gamma(r_1-1)+\left[\chi(b+2\Gamma)-b\right](r_2-1)\right\} . \tag{10b}$$

As is obvious, the stationary solution (E_1,E_2) will exist only if E_1^2 and E_2^2 are simultaneously positive, i.e., if e_3 and c_3 are simultaneously negative. Since we consider the pumps r_1 and r_2 as the main control parameters, it is convenient to represent the different zones of existence of (E_1,E_2) on the plane $\langle(r_1-1),(r_2-1)\rangle$. To make the analysis of the physical mechanisms responsible for the amplification of the radiation easier, we will distinguish four cases according to the value of χ: (i) $\chi<b/(b+2\Gamma)$; (ii) $b/(b+2\Gamma)<\chi<1$; (iii) $1<\chi<(b+2\Gamma)/b$; and (iv) $\chi>(b+2\Gamma)/b$.

Figure 2 shows the zones of existence of the two-mode solution (E_1,E_2) on the plane $\langle(r_1-1),(r_2-1)\rangle$ for $b=\Gamma$ and for a value of χ corresponding to the domain (i) above indicated, $\chi=0.25$. In this figure (E_1,E_2) exists only in the regions marked with roman numerals I, II, and III. The regions of existence of the other stationary solutions (0,0), $(E_1,0)$, and $(0,E_2)$ have not been depicted: the trivial solution exists in all the plane, while $(E_1,0)$ exists in all the right half-plane ($r_1>1$) and $(0,E_2)$ in all the upper half-plane ($r_2>1$). This means that there is coexistence of several solutions. Nevertheless, as will be shown later, bistability or multistability among them does not occur.

In the case of Fig. 2 ($\chi=0.25$) the system's efficiency is larger for the amplification of the field E_2 (upper transition) than for the field E_1 (lower transition). As is seen in Eq. (8d) the population inversion corresponding to the lower transition D_1 is always positive for this value of χ. A first feature evident in the figure is the existence of a region in the fourth quadrant ($r_1>1$, $r_2<1$) for which the two-mode solution exists. This means that the field E_2 can be generated together with the field E_1 [solution (E_1,E_2)] with a pump scheme ($r_2<1$, even r_2 negative) for which the field E_2 cannot be generated alone [solution

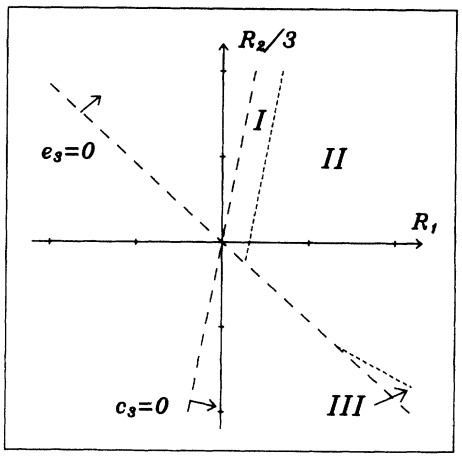

FIG. 2. Phase diagram on the plane defined by the pump parameters $R_1=r_1-1$ and $R_2=r_2-1$, showing the domains I, II, and III of the two-field steady solution (E_1,E_2), for $b=\Gamma$ and $\chi=0.25$. Domain I: positive inversions in the upper and lower transitions. Domain II: negative upper inversion but positive two-photon inversion. Domain III: absence of two-photon inversion (only lower inversion is positive). The functions c_3 and e_3 are defined in Eqs. (10). The arrows indicate the sense in which c_3 and e_3 are negative (condition for existence of the two-field solution). Each division in both R_1 and R_2 axes equals 5 units.

$(0,E_2)$ requires $r_2>1$].

A second important feature is the existence of regions where some of the population inversions are negative. This is marked in the figure with the numerals I (positive inversions), II (negative upper inversion, $D_2<0$, but positive two-photon inversion between levels 2 and 1), and III (absence of two-photon inversion). The existence of region III, where the upper level is less populated than any of the lower levels in steady state, is a demonstration of the role played by the *cooperation* between pump mechanisms mentioned above, that lead to a noninverted steady-state population distribution which is accompanied by emission rather than by absorption. However, one must not think of this kind of *emission without inversion* as an example of *lasing (amplification) without inversion* in the usual sense [14], since the two-mode solution of this cascade laser model needs positive inversion between the upper level 2 and the lower level 1 (two-photon inversion) in the absence of fields.

Some authors have recently suggested cascade schemes for the generation of laser radiation without inversion, considering one of the fields as an injected pump field (they are not cascade lasers) [15,16]. This shows the capacity of this kind of systems to exhibit nonreciprocal absorption and emission profiles, which are at the origin of these kinds of behavior. At difference with other inversionless laser schemes in which there is a positive inversion between a bare state and a state dressed by the preexistent (external) field [17], in the cascade laser this is not the case. It is easy to see that, in region III, the upper level 2 has less population than any (arbitrary) linear combination of the two lower levels 0 and 1 corresponding either to a dressing by the field E_1 or to any other combination.

There is an additional outstanding feature in Fig. 2. Note that there is a small region for which (E_1,E_2) is not generated in spite of the positive value of r_2 and r_1 and the positive value of all three population inversions [zone between the line $c_3=0$ and the (r_2-1) positive axis]. This *inversion without lasing* behavior is an example of *interference* between pump mechanisms, as opposed to the *cooperation* shown above. These phenomena are planned to be investigated in more detail in a forthcoming paper.

When χ increases reaching the domain $b/(b+2\Gamma)<\chi<1$ the slope of the $c_3=0$ line in Fig. 2 becomes negative, so that the domain I penetrates partially the second quadrant (the small region in the first quadrant for which (E_1,E_2) was not generated disappears). In the very particular case $\chi=1$, the inversions are equal to 1 in all the plane and coherent two-photon processes are absent in average, as mentioned above. This leads to a unique region (region I) with respect to the inversions (regions II and III disappear). Finally, in the domains (iii) and (iv) above there is an equivalence with the domains (ii) and (i), respectively, under the symmetry of Eqs. (4).

IV. LINEAR STABILITY ANALYSIS

Now we analyze in detail the stability of the different stationary solutions given in the preceding section by means of a linear stability analysis (LSA). In particular, we study how the system changes from one to another of these solutions and how some of them destabilize into a dynamic solution.

According to the standard technique for LSA, linearization of Eqs. (4) around the stationary solution which is going to be analyzed leads to the general expression

$$\frac{d}{d\tau}\mathbf{u}(\tau)=L\,\mathbf{u}(\tau)\ , \tag{11a}$$

where $\mathbf{u}(\tau)$ is the so-called local vector and its components

$$u_i(\tau)=x_i(\tau)-\bar{x}_i \tag{11b}$$

are the variables x_i $(D_2,P_2,E_2,D_1,P_1,E_1,Q)$ shifted to their stationary value $\bar{x}_i$ and

$$L=\begin{vmatrix} -b & -4\bar{E}_2 & -4\bar{P}_2 & 0 & \frac{2}{\chi}\bar{E}_1 & \frac{2}{\chi}\bar{P}_1 & 0 \\ \bar{E}_2 & -1 & \bar{D}_2 & 0 & 0 & \frac{1}{\sqrt{\chi}}\bar{Q} & \frac{1}{\sqrt{\chi}}\bar{E}_1 \\ 0 & \sigma_2 & -\sigma_2 & 0 & 0 & 0 & 0 \\ 0 & 2\chi\bar{E}_2 & 2\chi\bar{P}_2 & -b & -4\bar{E}_1 & -4\bar{P}_1 & 0 \\ 0 & 0 & -\sqrt{\chi}\bar{Q} & \bar{E}_1 & -1 & \bar{D}_1 & -\sqrt{\chi}\bar{E}_2 \\ 0 & 0 & 0 & 0 & \sigma_1 & -\sigma_1 & 0 \\ 0 & -\sqrt{\chi}\bar{E}_1 & \frac{1}{\sqrt{\chi}}\bar{P}_1 & 0 & \frac{1}{\sqrt{\chi}}\bar{E}_2 & -\sqrt{\chi}\bar{P}_2 & -\Gamma \end{vmatrix}\ . \tag{11c}$$

Let us proceed to determine the conditions under which the matrix L provides eigenvalues with a positive real part (condition for destabilization) for the different stationary solutions.

A. LSA of solution (0,0)

Diagonalization of the matrix L, when $\bar{x}_i$ takes the values given in Eqs. (5), leads to the following characteristic equation:

$$(\lambda+b)^2(\lambda+\Gamma)[\lambda^2+(\sigma_2+1)\lambda-\sigma_2(r_2-1)]\times[\lambda^2+(\sigma_1+1)\lambda-\sigma_1(r_1-1)]=0\ , \tag{12}$$

where λ denotes the eigenvalue. From Eq. (12) two independent conditions for the destabilization of the solution (0,0) through a pitchfork bifurcation (PB) are ob-

tained: $r_2>1$ *or* $r_1>1$. These conditions coincide with those for the existence of the single-field solutions $(0,E_2)$ and $(E_1,0)$, respectively. Thus the trivial solution bifurcates through a PB to $(0,E_2)$ at $r_2=1$ if $r_1<1$, or to $(E_1,0)$ at $r_1=1$ if $r_2<1$. Bifurcation of (0,0) to the two-field solution (E_1,E_2) is possible only in the very particular case $r_1=r_2=1$, in which, as will be seen below, both single-field solutions are unstable.

B. LSA of solution $(0,E_2)$

In this case the characteristic polynomial reduces to

$$(\lambda+b)A_2B_2=0\ , \tag{13a}$$

with

$$A_2=\lambda^3+(\sigma_2+b+1)\lambda^2+b(\sigma_2+r_2)\lambda+2b\sigma_2(r_2-1)\ , \tag{13b}$$

$$B_2=\lambda^3+c_1\lambda^2+c_2\lambda+c_3\ , \tag{13c}$$

$$c_1=\sigma_1+\Gamma+1\ , \tag{13d}$$

$$c_2=\Gamma(\sigma_1+1)-\sigma_1(r_1-1)+\frac{b-2\chi\sigma_1}{4}(r_2-1)\ , \tag{13e}$$

and c_3 is given by (10b).

Again, as in Sec. IV A, due to the factorized form of Eq. (13a) one can obtain thresholds for instabilities either making $A_2=0$ or $B_2=0$. The polynomial A_2 is obtained from the submatrix in L affecting the variables (D_2,P_2,E_2), as well as B_2 is obtained from the submatrix affecting (P_1,E_1,Q). Consequently, the repulsive directions which will appear at the thresholds provided by $A_2=0$ will mainly affect the variables (D_2,P_2,E_2), whereas those provided by $B_2=0$ will mainly affect the variables (P_1,E_1,Q). Let us analyze separately the conditions $A_2=0$ and $B_2=0$.

Polynomial A_2 is identical to that obtained in the Lorenz-Haken model [13]. As is well known, this equation leads to a Hopf bifurcation (HB) at $r_2=r_2^{\mathrm{HBL}}$, where

$$r_2^{\mathrm{HBL}}\equiv\frac{\sigma_2(\sigma_2+b+3)}{\sigma_2-b-1}\ , \tag{14a}$$

whenever

$$\sigma_2>\sigma_2^L\equiv b+1\ , \tag{14b}$$

which is known as the "bad cavity" condition. Thus this HB (in the following to be referred to as HBL) depends only on σ_2 and b.

As A_2, polynomial B_2 is cubic and provides a pitchfork bifurcation (PB) and a Hopf bifurcation. In order to make clear the sequence of bifurcations, let us assume r_2 to be the main control parameter [remember that $r_2>1$ since we are analyzing the solution $(0,E_2)$]. The PB appears at $c_3=0$, which explicitly reads

$$r_2=r_2^{\mathrm{PB}}\equiv1+\frac{4\Gamma}{b-\chi(b+2\Gamma)}(r_1-1)\ , \tag{15}$$

and is independent of the cavity losses. Solution $(0,E_2)$ will be unstable whenever $c_3<0$. In order to clarify this last requirement two cases must be distinguished depending on the value of χ: (i) Whenever $\chi<b/(b+2\Gamma)$ the solution $(0,E_2)$ is unstable for $r_2<r_2^{\mathrm{PB}}$. This situation coincides with the existence of the solution (E_1,E_2), as can be easily seen in Eqs. (10) (see Fig. 2). (ii) When $\chi>b/(b+2\Gamma)$ the solution $(0,E_2)$ is unstable whenever $r_2>r_2^{\mathrm{PB}}$. Again this condition coincides with the existence of the solution (E_1,E_2) (see Sec. III D), except when $\chi>(b+2\Gamma)/b$. In this last situation, where $r_1>1$ implies $r_2^{\mathrm{PB}}<0$, what occurs is that solution $(0,E_2)$ is born unstable since any value of $r_2>1$ [necessary condition for the existence of $(0,E_2)$] causes c_3 to be negative.

The above analysis can be summarized as follows: solution $(0,E_2)$, when bifurcating through a PB, gives rise to solution (E_1,E_2). There is no domain of bistability between these two solutions.

Let us consider now the Hopf bifurcation provided by polynomial B_2. This bifurcation (to be referred to as HBC in the following) occurs at $c_1c_2-c_3=0$, which explicitly reads

$$r_2=r_2^{\mathrm{HBC}}\equiv1+\frac{4(\sigma_1+1)}{2\sigma_1+2-b}\frac{r_1^*-r_1}{\chi-\chi^*} \tag{16}$$

with the definitions

$$r_1^*\equiv1+\frac{\Gamma(\Gamma+\sigma_1+1)}{\sigma_1}\ , \tag{17a}$$

$$\chi^*\equiv\frac{b(\Gamma+1)}{\sigma_1(2\sigma_1+2-b)}\ . \tag{17b}$$

Notice that at difference with r_2^{HBL}, which tends to infinity as σ_2 does, r_2^{HBC} tends to a finite value when σ_1 goes to infinity: $r_2^{\mathrm{HBC}}(\sigma_1\to\infty)=1+2(\Gamma-r_1-1)/\chi$.

Again, two cases must be distinguished, depending on the value of χ. If $\chi>\chi^*$ the oscillations will develop for $r_2>r_2^{\mathrm{HBC}}$ (independently of the pump r_1). On the contrary, if $\chi<\chi^*$ the HBC will exist only for $r_1>r_1^*$ and the oscillations will appear whenever $r_2<r_2^{\mathrm{HBC}}$. Nevertheless, this last region of instabilities (when existing) is extremely small and therefore is of no practical importance.

It is to be recalled that this Hopf bifurcation affects variables which are null in steady state (E_1, P_1, and Q). Interestingly enough, the field E_1 can be dynamically amplified [in a way that will be shown in Fig. 3(b)] before reaching the threshold for its stationary amplification in the two-field configuration (r_2^{PB}).

Obviously the stationary solution $(0,E_2)$ will bifurcate either at r_2^{PB}, or r_2^{HBC} or r_2^{HBL}, depending on which of these thresholds is first reached. Codimension-2 and even codimension-3 points [18] can appear if these thresholds coincide. In Sec. V these features will be exemplified for some particular cases.

C. LSA of solution $(E_1,0)$

In this case the pump parameter $r_1>1$. The characteristic polynomial reduces to

$$(\lambda+b)^2(\lambda+\Gamma)A_1B_1=0\ , \tag{18}$$

where A_1 and B_1 are polynomials similar to A_2 and B_2 in Eqs. (13) except for the changes $(1\rightarrow 2,\ \chi\rightarrow 1/\chi)$. Thus no particular analysis must be made in this case since all the considerations made in Sec. IV C for $(0,E_2)$ are valid for $(E_1,0)$ *mutatis mutandi,* due to the symmetry of Eqs. (4).

D. LSA of solution (E_1,E_2)

For the two-field solution the corresponding polynomial is of seventh order, so that no general analytical expressions can be obtained. Only in the very particular case in which both transitions have the same parameters ($\sigma_1=\sigma_2$ and $\chi=1$) and equal pumping ($r_1=r_2$), the seventh-order polynomial is factorized into fourth- and third-order ones. This case has been recently reported by us in Ref. [6], where a LSA has been performed and the associated dynamic regimes have been characterized, and in Ref. [19], where the influence of parameter variations on the thresholds has been discussed. We refer the reader to these papers.

V. SPECIAL CASES

It is clear that most of the bifurcations discussed in the preceding section do not admit a simple viewing. This fact is even more acute in the case of the solution in which both fields are present, (E_1,E_2), since no analytical expressions are available in general. Thus in this section we will concentrate on how the sequence of possible bifurcations is produced. Given the large number of free parameters, it will be necessary to fix some of them.

In our model the relaxation rates of both induced dipoles have been taken to be equal. Although the relaxation rate of the two-photon coherence Γ could be different than those of the dipoles, one can assume Γ to be similar to those in many cases. Then we will take $\Gamma=1$ along this section.

On the other hand, the normalized population relaxation rate b (which was taken to be equal for the three levels) can vary from 0 to 1. For the sake of simplicity we have chosen $b=1$, which is equivalent to considering the dephasing collisions to be negligible. In any case we have verified that variations in the value of b do not affect qualitatively the results we present next.

One additional simplification must be made. It concerns the value of the cavity losses σ_1 and σ_2. In order to make the results easily understandable we have chosen $\sigma_1=\sigma_2\equiv\sigma$. This condition can be fulfilled with a double-ring configuration, as that reported in Ref. [4(a)]. Even this limitation can be reasonable in the case of only one ring if the optical elements arranged along it do not affect both fields quite differently. In any case fixing both cavity losses to the same value seems to be a natural first step in studying the system. Specific work on the influence of different cavity losses for each field will be reported elsewhere.

Summarizing, in the present section we have made the election

$$b=\Gamma=1\ ,\quad \sigma_1=\sigma_2\equiv\sigma\ ,$$

so that we keep as free parameters the pumps r_1 and r_2, the common cavity losses σ, and the relative efficiency for amplification of the fields E_1 and E_2, χ.

Since four parameters are difficult to handle simultaneously, we have divided the study of the different bifurcations into three subsections. In the first (Sec. V A) and the second (Sec. V B) two fixed pump schemes are set and the bifurcations are discussed as a function of cavity losses σ and relative efficiency χ. In Sec. V C no particular pump scheme is considered and the bifurcations are studied for a fixed value of σ.

A. Case $r_1=0$

The electron $r_1=0$ corresponds to pumping only the upper level 2 (or, mathematically, that levels 0 and 1 are equally pumped). This pump scheme prevents the existence of the solution $(E_1,0)$. Thus only the bifurcations affecting (0,0), $(0,E_2)$, and (E_1,E_2) must be considered. By increasing r_2 the trivial solution loses its stability at $r_2=1$, value at which solution $(0,E_2)$ emerges. In turn, this solution can undergo three different types of bifurcations, namely, PB, HBC, and HBL, whose respective thresholds and parameter conditions are

$$r_2^{\mathrm{PB}}=1+\frac{4}{3\chi-1}\ , \tag{19a}$$

$$\chi>\tfrac{1}{3}\ , \tag{19b}$$

$$r_2^{\mathrm{HBL}}=1+\frac{\sigma^2+3\sigma+2}{\sigma-2}\ , \tag{20a}$$

$$\sigma>\sigma^L=2\ , \tag{20b}$$

$$r_2^{\mathrm{HBC}}=1+\frac{8(\sigma+1)^2}{\chi\sigma(2\sigma+1)-2}\ , \tag{21a}$$

$$\sigma>\sigma^c\equiv\tfrac{1}{4}(\sqrt{1+16/\chi}-1)\ . \tag{21b}$$

This means that $(0,E_2)$ will become unstable for r_2 greater than any of these thresholds. Equation (20b) is the bad-cavity condition for the HBL bifurcation in the present case. On the other hand, condition (21b) holds for the HBC bifurcation. Note that the value of σ^c can be smaller than that of σ^L, and r_2^{HBC} can also be smaller than r_2^{HBL}. Thus an interesting conclusion is that *in the cascade laser neither the bad-cavity condition nor the Lorenz second threshold need to be reached in order to obtain instabilities.* To this respect, Eqs. (16) and (17) show that, if we let σ_1 and σ_2 be different, the smallest value of σ_1 allowing one to reach the HBC instability threshold arbitrarily approaches zero as the population relaxation rate b does.

Obviously only the lower of the Hopf bifurcation thresholds of Eqs. (20a) and (21a) makes sense, whenever the pitchfork bifurcation r_2^{PB} [Eq. (19a)] is not reached. If r_2^{PB} is first trespassed none of the Hopf bifurcations exist since the stationary solution $(0,E_2)$ transforms into the stationary solution (E_1,E_2) and therefore the possible instabilities should be analyzed from this last stationary

solution. This operation has to be made numerically, as pointed out above.

Figures 3 and 4 illustrate the sequence in which bifurcations appear, for different values of χ. Figure 3 shows the dependence of the thresholds on σ for the case $\chi=\frac{1}{3}$. For this value the condition (19b) is not fulfilled and consequently the only two thresholds to be considered here are r_2^{HBL} and r_2^{HBC}. The two curves representing these thresholds intersect, giving rise to a codimension-2 (CO-2) point. For values of σ larger than that corresponding to the CO-2 point ($\sigma_{\mathrm{CO\text{-}2}}$) the curve r_2^{HBC} is below r_2^{HBL}, whereas the contrary occurs for $\sigma<\sigma_{\mathrm{CO\text{-}2}}$ (obviously when r_2 is increased the curve first reached is the one that determines the actual bifurcation of the analyzed stationary solution). In order to illustrate how these two bifurcations affect the stationary solution $(0,E_2)$, Figs. 3(b) and 3(c) show the evolution of the fields near the bifurcation point when either r_2^{HBC} or r_2^{HBL} are trespassed, respectively.

Figure 3(b) shows the time traces of the fields corresponding to the limit cycle that appears at the HBC point. The field E_1, which was null below the bifurcation point, is now generated with zero mean amplitude and 100% intensity modulation. This modulation slightly affects the strong field E_2, which becomes weakly modulated at twice the frequency (the intensity, however, has the same modulation). This can be interpreted as a result of the "slaving" of E_2 by E_1, P_1, and Q, since as shown above HBC comes from the subspace defined by these three variables.

Figure 3(c) shows the long-term behavior of the system when the HBL point is trespassed. It is apparent that the field E_2 evolves quite similarly to a typical Lorenz chaos [1], although with some differences due to the presence of the other field E_1. These small differences with respect to Lorenz behavior are apparent in Fig. 3(d), which shows the peak-to-peak map for the intensity $I_2=E_2^2$. The typical Lorenz "cusp map" appears slightly blurred due to the influence of the field E_1. The field E_1, however, cannot follow the fast and strong variations of E_2 and exhibits a slower and more erratic time evolution [Fig. 3(c)], which gives rise to the non-Lorenz map of Fig. 3(e).

The outstanding feature of these two Hopf bifurcations is that they allow the field E_1 to be generated in spite of its null stationary value.

In the Appendix it is shown by means of a nonlinear analysis that *the small-amplitude oscillatory solutions emerging at the Hopf bifurcation points are supercritical (stable) for HBC and subcritical (unstable) for HBL.* Particularly, it is demonstrated analytically that the equations governing the stability of the periodic solutions which bifurcate at r_2^{HBL} coincide with those corresponding to the two-level single-mode (Lorenz-Haken) laser [20].

When $\chi>\frac{1}{3}$ [condition (19b)], the PB which did not exist in the preceding case appears. The larger is χ, the smaller the corresponding threshold r_2^{PB} becomes. This is illustrated in Figs. 4(a), 4(c), and 4(e), where the three thresholds are shown for increasing values of χ ($\chi=0.424\,428\,9\ldots$, 0.44, and 0.5, respectively).

The existence of r_2^{PB} leads to the appearance of a new CO-2 point which is given by the intersection between the r_2^{PB} and r_2^{HBC} lines [Fig. 4(c)]. As χ is increased, this CO-2 point occurs for decreasing values of r_2. For a certain value of χ ($\chi_{\mathrm{CO\text{-}3}}$), this CO-2 point becomes a CO-3 point since r_2^{PB} intersects simultaneously r_2^{HBC} and r_2^{HBL} [Fig. 4(a)].

For $r_2>r_2^{\mathrm{PB}}$, the stationary solution (E_1,E_2) appears. As stated above, its stability analysis has to be performed numerically. Figure 4(b) shows both the analytical thresholds for $(0,E_2)$ (which are physically meaningless for $r_2>r_2^{\mathrm{PB}}$) and the numerical ones for (E_1,E_2) (lines with dots). Notice how these new thresholds separate from r_2^{HBC} and r_2^{HBL} as σ does from $\sigma_{\mathrm{CO\text{-}3}}$. Note also the existence of another CO-2 point given by the crossing of the two Hopf bifuractions affecting (E_1,E_2).

For $\chi>\chi_{\mathrm{CO\text{-}3}}$ the CO-3 point becomes again CO-2 point [Figs. 4(c) and 4(d)] up to a certain value of χ ($\chi=0.5$) for which it disappears since the r_2^{PB} line remains always below r_2^{HBC} [Figs. 4(e) and 4(f)]. Although in this last case the curves r_2^{HBC} and r_2^{HBL} do not make physical sense, it is worth noting that their position and shape are quite similar to those of the curves describing the Hopf bifurcations associated to the two-field solution [lines with dots in Figs. 4(e) and 4(f)]. Nevertheless, as χ is further increased, the quantitative differences between the single-field and two-field stability curves become more evident. An additional consequence of increasing χ is to bring r_2^{PB} closer to the value $r_2=1$, the value at which $(0,E_2)$ appears. This means that the domain of stability of this last solution decreases. This is natural since increasing χ corresponds to favoring the amplification of the field E_1 more and more.

Summarizing the dependence on χ, three main domains can be considered: $\chi<\frac{1}{3}$, for which $(0,E_2)$ destabilizes through a Hopf bifurcation (r_2^{HBC} or r_2^{HBL}); $\chi>\frac{1}{2}$, for which it destabilizes through a pitchfork bifurcation (r_2^{PB}), leading to the solution (E_1,E_2) (which is affected by Hopf bifurcations); and $\frac{1}{3}<\chi<\frac{1}{2}$, for which the PB occurs for small cavity losses σ and the HB occurs for larger values of σ. This last domain in χ is the one that shows a greater variety of bifurcations and several types of multicodimensional points.

B. Case $r_2=0$

This case corresponds physically to equally pumping the upper and intermediate molecular levels, with the result of no net pumping of the upper transition 2-0 ($r_2=0$). Although this pump scheme is, in principle, of more difficult implementation, it represents the complementary case of the preceding one in which we had $r_1=0$. In fact, due to the symmetry properties of Eqs. (4) the LSA provides here the same results as in Sec. V A, changing χ by $1/\chi$, r_1 by r_2, and taking into account that the analyzed solution is $(E_1,0)$ in the present case instead of $(0,E_2)$. The numerical analysis of the solution (E_1,E_2) provides, obviously, the same results also.

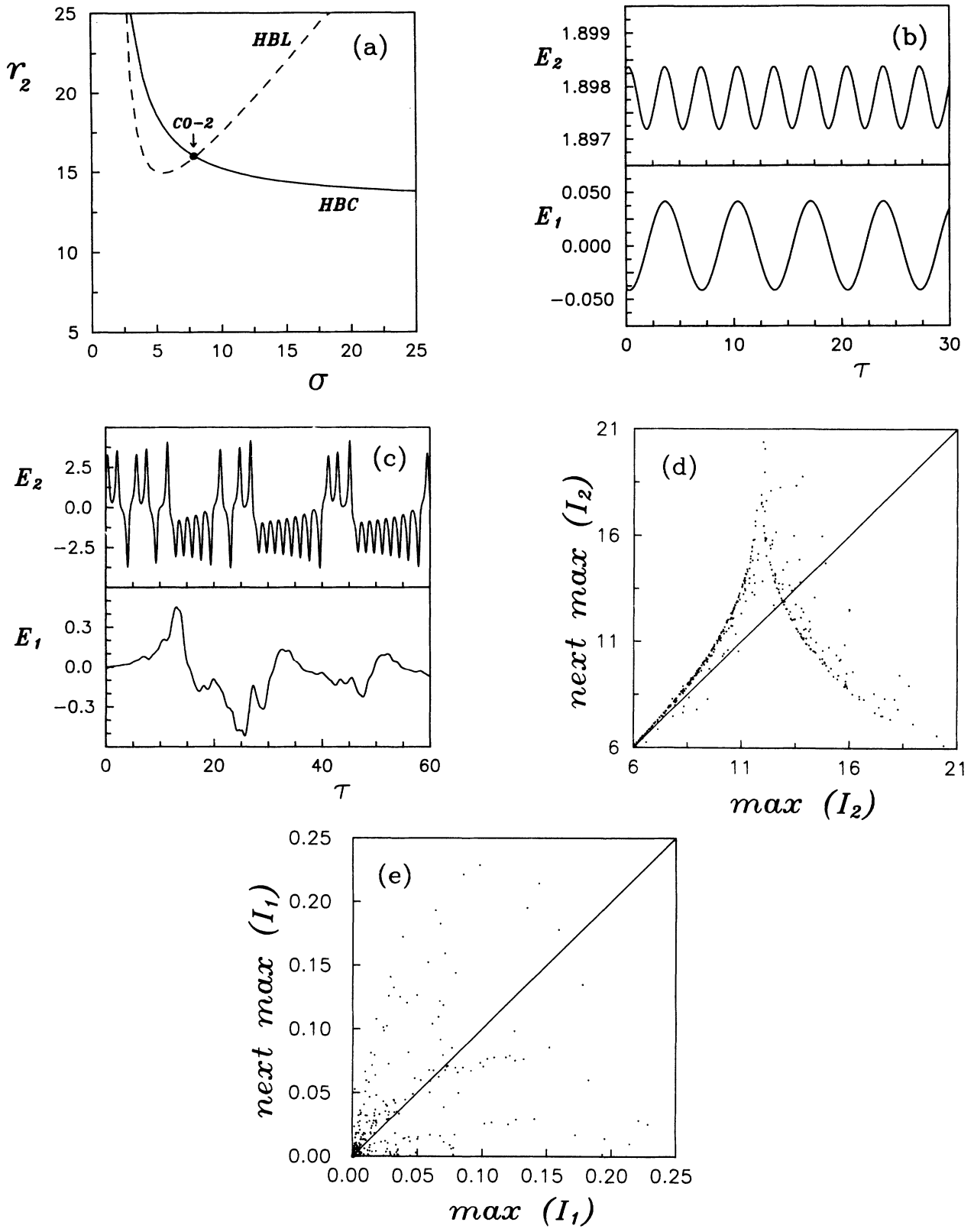

FIG. 3. (a) Upper transition pump threshold r_2 as a function of cavity losses $\sigma_1=\sigma_2=\sigma$ for the "Lorenz" Hopf bifurcation HBL (dashed line) and the "cascade" Hopf bifurcation HBC (continuous line) affecting the $(0,E_2)$ solution for $r_1=0$, $\chi=\frac{1}{3}$, and $b=\Gamma=1$. In this case the two-field steady solution does not exist. The intersection of the two lines defines a codimension-2 point. (b) Time evolution of the fields E_1 and E_2 for r_2 slightly above HBC ($\sigma=10$, $r_2=15.4$). (c) Same as (b) but for r_2 slightly above HBL ($\sigma=5$, $r_2=15.05$). (d) Height of each peak of the intensity $I_2=E_2^2$ in (c) vs height of the preceding peak (intensity map). (e) The same for the intensity $I_1=E_1^2$.

C. Case $r_1 \neq 0 \neq r_2$

In this subsection we do not consider any particular pump scheme. Thus we let both r_1 and r_2 be free control parameters. In Fig. 5 we show, on the plane (r_1-1, r_2-1), all the possible bifurcation curves affecting the single- and two-field solutions, for $\sigma=5$ and $\chi=0.25$ (a), 0.5 (b), 0.75 (c), and 1.0 (d). The shadowed regions correspond to the domains of stability of the three stationary solutions (see figure caption). Note how the Hopf bifurcations affecting the one-mode solutions $(0,E_2)$—HBC and HBL—and $(E_1,0)$—HBL—connect in a continuous way with those affecting the two-mode solution (E_1,E_2)—HB and HB′—which have been numerically computed. Note also how the bifurcation diagram symmetrizes with respect to the axis $r_1=r_2$, as χ approaches 1. Since $\chi \leq 1$ in these figures the bifurcation HBC affects only the solution $(0,E_2)$ [if $\chi \geq 1$, HBC would affect $(E_1,0)$ due to the symmetry properties of Eqs. (4).] Let us point out finally that if one considers a particular pump scheme given by a fixed proportion of the pumping rates of the three molecular levels, $\lambda_2:\lambda_0:\lambda_1$, a variation in the pump strength results in moving along the straight line

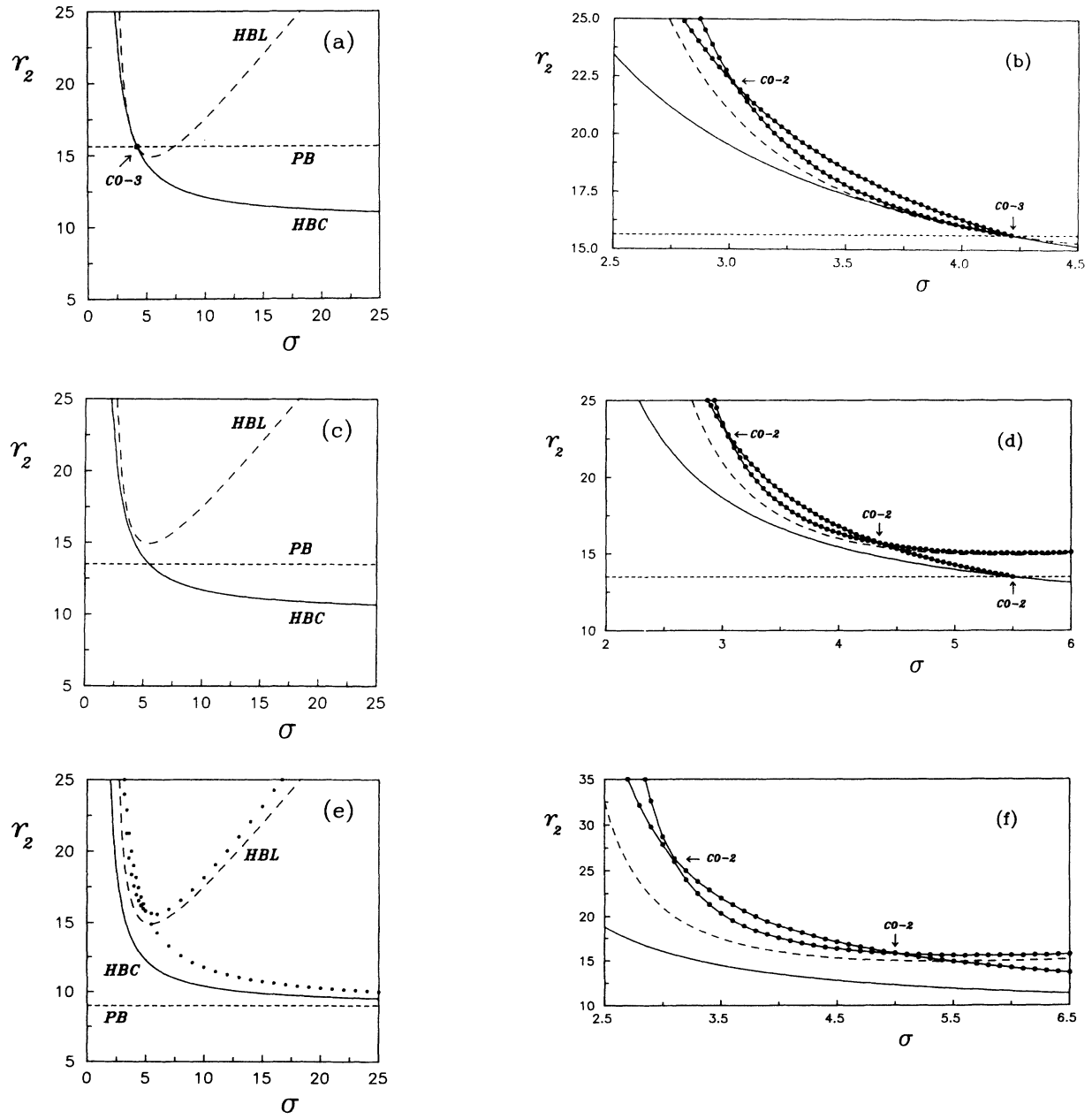

FIG. 4. The same as in Fig. 3(a), for (a),(b) $\chi=0.424\,428\,9\ldots$; (c),(d) $\chi=0.44$; and (e),(f) $\chi=0.5$. The line PB describes the pitchfork bifurcation transforming the solution $(0,E_2)$ into (E_1,E_2). (a) CO-3: codimension-3 point. (b),(d,)(f): the continuous lines with dots represent the thresholds for the two Hopf bifurcations affecting the two-field solution [the dotted lines in (e) have the same meaning].

$$r_2=\frac{\lambda_2-\lambda_0}{\lambda_0-\lambda_1}\frac{1}{\chi}r_1 \tag{22}$$

in these diagrams. As an example, the cases considered in the previous subsections correspond to moving along the vertical line $r_1=0$ ($R_1=-1$) and along the horizontal line $r_2=0$ ($R_2=-1$), respectively.

VI. DYNAMIC BEHAVIOR

Here we study the dynamic solutions that Eqs. (4) can exhibit near and far from the steady points. This is done for the case reported in Sec. V A, i.e., for $r_1=0$ with $b=\Gamma=1$ and $\sigma_1=\sigma_2=\sigma$. We will consider the subcases $\chi=0.3$ and $\chi=0.6$, which correspond to dynamics linked to the single-field solution $(0,E_2)$ and the two-field solu-

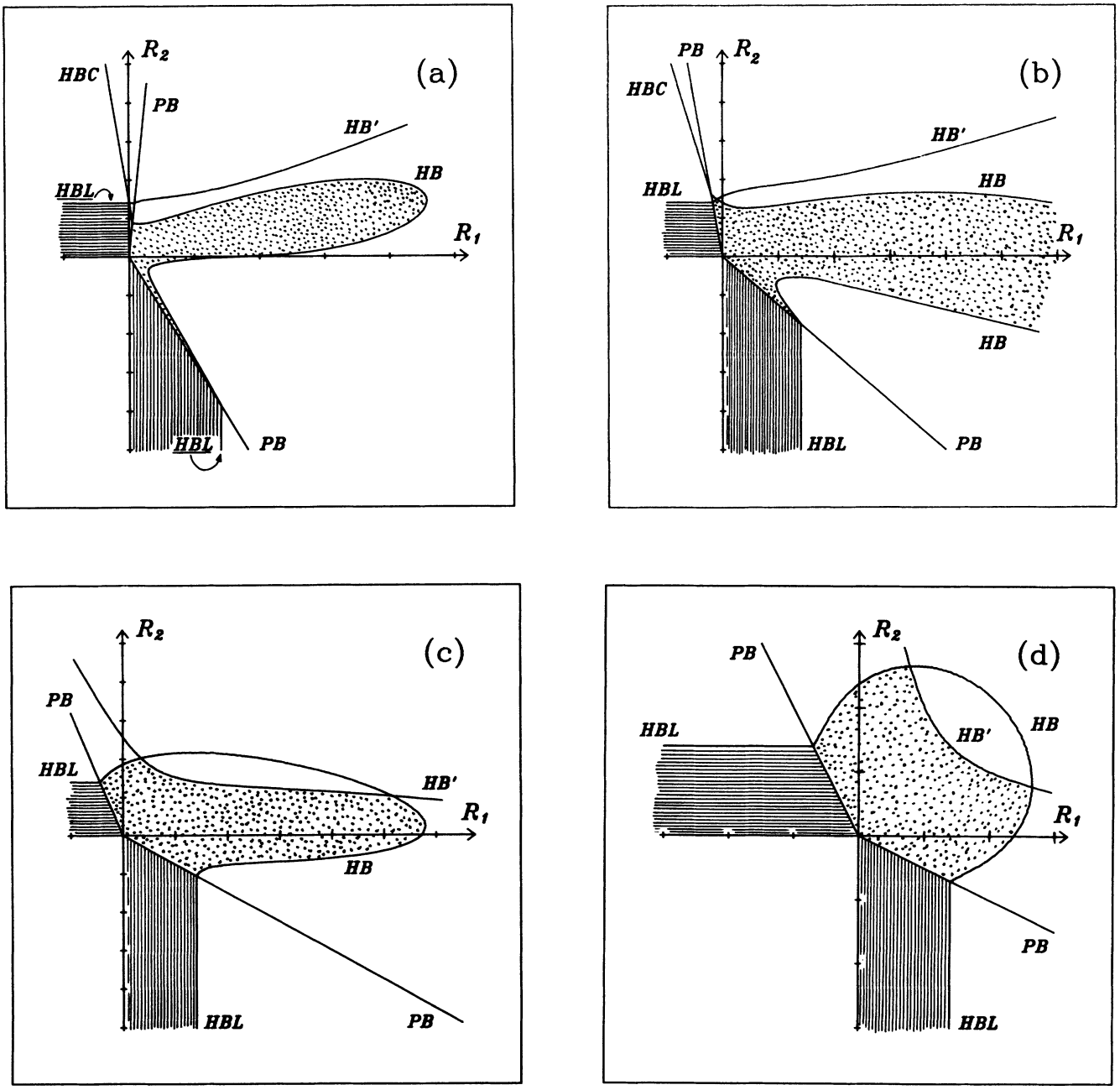

FIG. 5. Phase diagrams on the plane (R_1,R_2) showing the different bifurcation lines for $\sigma_1=\sigma_2=\sigma=5$, $b=\Gamma=1$, and $\chi=0.25$ (a), 0.5 (b), 0.75 (c), and 1.0 (d). The shadowed regions correspond to the stability domains of the stationary solutions $(E_1,0)$ (vertical shadow), $(0,E_2)$ (horizontal shadow), and (E_1,E_2) (dotted shadow). PB: pitchfork bifurcation transforming single-field into two-field solutions. HBC and HBL: "cascade" and "Lorenz" Hopf bifurcations affecting the single-field solutions. HB and HB': Hopf bifurcations affecting the two-field solution. Each division in both R_1 and R_2 axes equals 10 units.

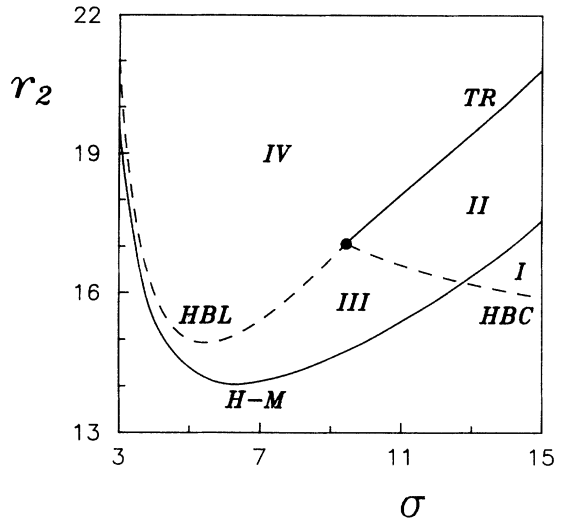

FIG. 6. Phase diagram showing the different domains of dynamic behavior corresponding to $\chi=0.3$ and the rest of parameters as in Fig. 3(a). H-M denotes the threshold for hard-mode excitation instabilities. Region I: periodic solution. Region II: generalized bistability between periodic and chaotic solutions. Region III: generalized bistability between steady-state $(0,E_2)$ and chaotic solutions. Region IV: chaotic solution. TR: narrow domain of quasiperiodic (torus T^2) behavior. The dot denotes the CO-2 point.

tion (E_1,E_2), respectively.

In Fig. 6 the main domains of dynamic behavior found for $\chi=0.3$ have been represented together with the threshold lines for HBL and HBC (dashed lines), which are the only bifurcations affecting the solution $(0,E_2)$ [Fig. 3(a)]. The dynamics have been investigated both with hard- and soft-mode excitations, i.e., solving Eqs. (4) for a given pump r_2 subject to initial conditions that correspond either to laser off, or to the solution found for a near value of r_2, respectively. When r_2 is continuously

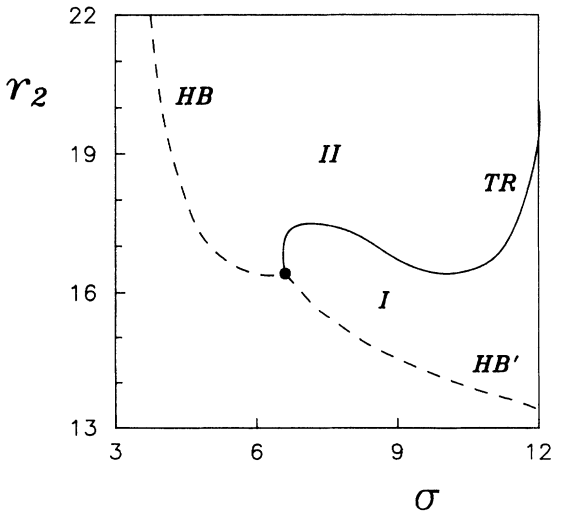

FIG. 7. The same as in Fig. 6, for $\chi=0.6$. HB and HB': threshold lines for the two Hopf bifurcations that affect the two-field solution. Region I: periodic behavior. Region II: chaotic behavior. TR: torus T^2.

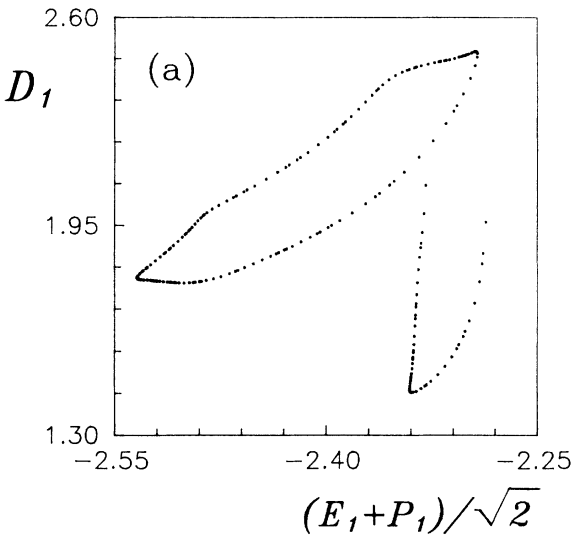

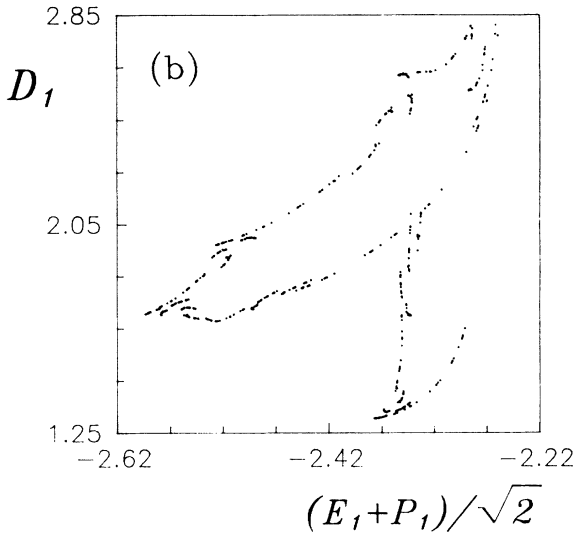

FIG. 8. Poincaré sections corresponding to the quasiperiodic motion indicated in Fig. 7 (line TR) for $\sigma=12$, before (a) and after (b) destabilization. The Poincaré section corresponds to (a) $r_2=20.160$ and (b) $r_2=20.185$.

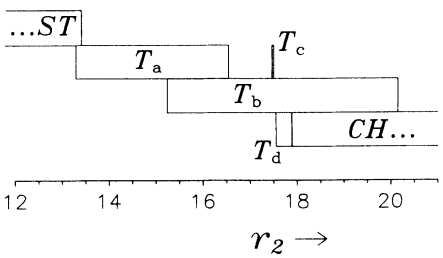

FIG. 9. Bifurcation diagram showing the different attractors appearing in the case of Fig. 7 as a function of the pump parameter r_2, for $\sigma=12$. ST: steady-state two-field solution. T_a, T_b, T_c, and T_d: periodic solutions appearing in region I of Fig. 7. CH: chaotic behavior.

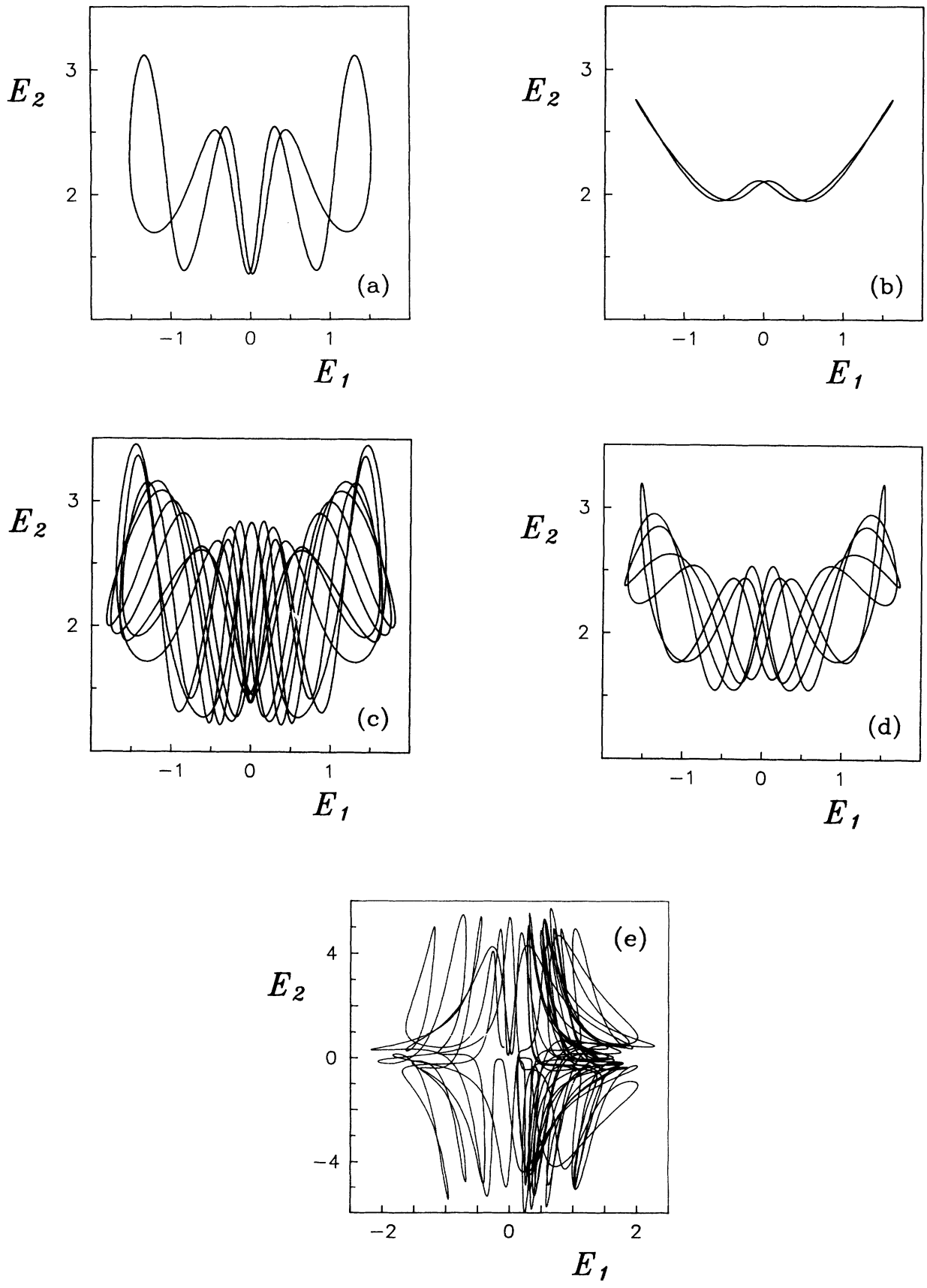

FIG. 10. Field portraits associated with the attractors (a) T_a, (b) T_b, (c) T_c, (d) T_d, and (e) CH shown in Fig. 9. $r_2=16.0$ (a), 17.0 (b), 17.5 (c), 17.7 (d), and 19.0 (e).

increased and soft-mode excitation is used the single-field solution is obviously stable until HBC or HBL is reached. If $\sigma < \sigma_{\text{CO-2}}$ (the CO-2 point is marked with a dot in the figure) a sudden transition to chaos occurs after HBL. If $\sigma > \sigma_{\text{CO-2}}$ the supercritical character of HBC causes the system to develop periodic oscillations around the steady solution. These oscillations grow in amplitude when r_2 is further increased up to the curve TR, at which a transition to a torus T^2 occurs. This quasiperiodic solution is extremely unstable and lasts only as much as a few hundredths in the pump parameter value giving rise to chaos (quasiperiodicity scenario [21]). Above the TR line no transition from chaotic to periodic behavior has been observed. When hard-mode excitation is used the threshold for instabilities is manifestly lowered (up to ca. $\frac{1}{8}$ reduction around the CO-2 point) indicating the existence of generalized bistability between the stationary solution $(0,E_2)$ and the chaotic attractor (region III) and between the periodic attractor and the chaotic one (region II). The curve H-M indicates the lowest value of r_2 at which chaotic dynamics is found with hard-mode excitation. In region I only periodic oscillations exist whereas only chaotic behavior is found in region IV. In this last region the chaos is approximately of Lorenz-type below and near the HBL line. An example of the temporal behavior obtained both in the periodic and chaotic regions has been shown in Figs. 3(b) and 3(c), respectively.

Next we study the dynamics for the case $\chi=0.6$. For this value of χ the first bifurcation reached by the $(0,E_2)$ solution is the pitchfork bifurcation at $r_2=6.0$. Therefore we must study the dynamics of the two-field solution (E_1,E_2). In Fig. 7 the dashed line denotes the threshold for destabilization of this solution. The dot marks a CO-2 point corresponding to the crossing of the two possible Hopf bifurcations HB and HB' this solution can undergo. As the HBL single-field bifurcation, the Hopf bifurcation line HB (low-σ domain in Fig. 7) is subcritical and gives rise to chaotic motion. The Hopf bifurcation line HB' (large-σ domain), however, is also subcritical, at difference from the supercritical character of HBC. The domain of generalized bistability reached by hard-mode excitation has not been plotted in Fig. 7 due to its smallness, particularly for $\sigma > \sigma_{\text{CO-2}}$. As for $\chi=0.3$ there are two main types of dynamic regimes: periodic (zone I) and chaotic (zone II), and the transition from one to another (line TR) also occurs through quasiperiodicity. In Fig. 8 this transition to chaos is exemplified by means of Poincaré sections that correspond to quasiperiodic motion on a torus T^2 before [Fig. 8(a)] and after [Fig. 8(b)] destabilization [22].

The dynamics in the periodic domain is much richer than in the preceding case. There are at least four different periodic attractors that can coexist, at least two at a time. Figure 9 shows a detailed bifurcation diagram of the system for $\sigma=12$ as the pump r_2 is varied. Domains of bistability between the different attractors are clearly observed. The periodic behavior denoted as T_a is the one which covers most of region I in Fig. 7. The other periodic attractors are denoted by T_b, T_c, and T_d, and exist over much smaller regions in parameter space. Concerning the last two attractors, they have been

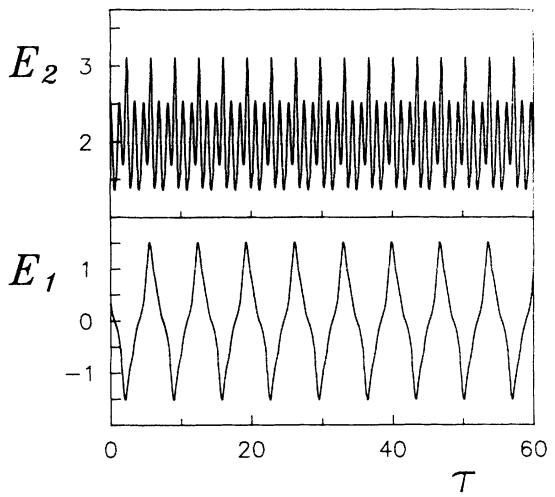

FIG. 11. Time evolution of the fields E_1 and E_2 for the attractor T_a shown in Fig. 10(a).

discovered just by hard-mode excitation: if the dynamics is initiated *from* the destabilization of the steady-state solution (E_1,E_2) (ST in the figure) then increasing r_2 leads to the sequence $T_a \rightarrow T_b \rightarrow$ chaos (CH in the figure), and T_c and T_d are not visited. The destabilization of each of these attractors has always been observed to be via T^2 tori. Examples of the dynamics associated to T_a, T_b, T_c, T_d, and CH are shown in Figs. 10(a)–10(e), respectively, by means of attractor projections on the field plane (E_1,E_2). Figure 11 shows the temporal series associated with one of these attractor projections. Note in these field portraits that the fields do not exhibit in general clear in-phase nor antiphase behavior, as another difference with respect to the multimode lasers. Only in the symmetric case $\chi=1$ and $r_1=r_2$ we found exact periodic antiphase dynamics, as reported in Ref. [6].

VII. CONCLUSIONS AND OUTLOOK

In this work we have performed a detailed analysis of the stationary solutions of a special class of two-field laser, namely, the nondegenerate cascade laser, in conditions of homogeneous broadening and exact resonance of the two fields with the corresponding atomic transitions. No bistability between steady-state solutions exists in this model in spite of the coexistence of one two-field and two single-field solutions.

In the two-field stationary solutions situations of cooperation or interference between pump mechanisms can lead to lasing without inversion (in a restricted sense, since *ab initio* two-photon positive inversion is required) or inversion without lasing, respectively.

The linear stability analyses have revealed the presence of two independent Hopf bifurcations that are shared by both single-field and two-field solutions. In the single-field case one of these HB's is exactly that of the single-mode two-level Lorenz-laser model (HBL) [1,13], and thus corresponds to one-photon processes. The other HB comes from two-photon processes (HBC) and allows for (i) instabilities below the second Lorenz threshold and without the bad-cavity condition [1,13]; and (ii) the "dy-

namic" generation of the field which is null in steady state, in conditions where the pump is insufficient for steady generation of this field (the field is created with 100% amplitude modulation). A nonlinear stability analysis has shown the subcritical character of the HBL bifurcation and the supercritical character of the HBC one.

Concerning the dynamics, we have found that the system exhibits chaotic behavior for a large domain in the parameter space; particularly, for moderate values of the cavity losses σ. For larger values of σ a wide domain of periodic behaviors appears in which several independent periodic attractors are present and can coexist. All the observed transitions from periodic to chaotic motion are via quasiperiodicity [21,24].

The work presented here should be continued mainly in two directions. Concerning the resonant cascade laser, the influence of different cavity losses for each mode is to be addressed, as well as the origin of the cooperativity or interference between pump mechanisms. On the other hand, the extension to nonresonant configurations is under progress, in particular, the study of the connection between the detuned cascade laser and the two-photon laser.

ACKNOWLEDGMENTS

Financial support from the Dirección General de Investigación Científica y Técnica (DGICYT), Spain, under Contract No. PB-89-0319-C03-03 and technical support from the Institut de Física Corpuscular (IFIC-UV computer center) are gratefully acknowledged.

APPENDIX

Here we determine the stability properties of the periodic orbits which bifurcate from the one-field steady solution $(0,E_2)$ at either of the two Hopf bifurcations (HBC or HBL) discussed in Sec. IV B. We basically follow the general treatment of Iooss and Joseph [25]; nevertheless, we think it is worth outlining the process since it can be useful to some readers, for we finally give the key quantities to be computed in order to determine the stability of the orbits, circumventing the actual construction of those periodic solutions, as opposed to other authors [20,26,27].

First we reduce the cascade laser model of Eqs. (4) to a local form,

$$\frac{d\mathbf{u}}{d\tau}=f(\mu;\mathbf{u}) , \tag{A1a}$$

where $\mathbf{u}$ is given in Eq. (11b), μ is the control parameter (which need not be specified to our purposes), and f is the function that gives the time derivative of $\mathbf{u}$. Expanding (A1a) in a Taylor series in powers of $\mathbf{u}$ around the steady solution ($\mathbf{u}=\mathbf{0}$), one obtains

$$\frac{d\mathbf{u}}{d\tau}=\underline{L}(\mu)\mathbf{u}+\frac{1}{2!}\mathbf{N}_2(\mu;\mathbf{u},\mathbf{u})\frac{1}{3!}+\mathbf{N}_3(\mu;\mathbf{u},\mathbf{u},\mathbf{u})+O(u^4) , \tag{A1b}$$

where $\underline{L}(\mu)$ is the matrix given by Eq. (11c) in which the stationary solution $\mathbf{u}=\mathbf{0}$ [$(0,E_2)$ given by Eq. (6) in our case] must be introduced, and

$$N_2^j(\mu;\mathbf{a},\mathbf{b})=\sum_{k,l=1}^{d}\left[\frac{\partial^2 f}{\partial u_k\partial u_l}\right]_{\mathbf{u}=0}a_k b_l ,$$

$$N_3^j(\mu;\mathbf{a},\mathbf{b},\mathbf{c})=\sum_{k,l,m=1}^{d}\left[\frac{\partial^3 f}{\partial u_k\partial u_l\partial u_m}\right]_{\mathbf{u}=0}a_k b_l c_m , \tag{A2a}$$

where $N_{2(3)}^j$ represents the jth component of vector $\mathbf{N}_{2(3)}$, d is the dimension of the problem (in our case $d=7$), and a_k, b_l, and c_m are the kth, lth, and mth components of arbitrary vectors $\mathbf{a}$, $\mathbf{b}$, and $\mathbf{c}$, respectively ($k,l,m=1,2,\ldots,d$). In our case,

$$\mathbf{N}_2(\mu;\mathbf{a},\mathbf{b})=\begin{bmatrix} -4(a_2b_3+a_3b_2)+2(a_5b_6+a_6b_5)/\chi \\ (a_1b_2+a_2b_1)+(a_6b_7+a_7b_6)\sqrt{\chi} \\ 0 \\ 2\chi(a_2b_3+a_3b_2)-4(a_5b_6+a_6b_5) \\ (a_4b_6+a_6b_4)-(a_3b_7+a_7b_3)\sqrt{\chi} \\ 0 \\ (a_3b_5+a_5b_3)/\sqrt{\chi}-(a_2b_6+a_6b_2)\sqrt{\chi} \end{bmatrix} , \tag{A2b}$$

which is a symmetric bilinear form, and $\mathbf{N}_3$ is null since no third-order nonlinearities exist in Eqs. (4) ($\mathbf{N}_3$ would be a symmetric trilinear form). Nevertheless, we maintain $\mathbf{N}_3$ explicitly, for it is necessary in general problems.

The linear part of Eq. (A1b) leads to the problem

$$\underline{L}(\mu)\zeta=\lambda(\mu)\zeta , \tag{A3a}$$

$$\zeta^{\dagger}\underline{L}(\mu)=\lambda(\mu)\zeta^{\dagger} , \tag{A3b}$$

$$\lambda(\mu)=\alpha(\mu)+i\beta(\mu) , \tag{A3c}$$

such that, at the Hopf bifurcation ($\mu=\mu_{\mathrm{HB}}$) $\lambda(\mu_{\mathrm{HB}})=i\omega_0$ and its corresponding eigenvectors will be called $\zeta=\boldsymbol{\wp}$ and $\zeta^{\dagger}=\boldsymbol{\ell}$. These vectors verify $\boldsymbol{\wp}\cdot\boldsymbol{\ell}^*=0$, and are chosen so that $\boldsymbol{\wp}\cdot\boldsymbol{\ell}=1$.

In order to determine the stability of the periodic solutions which bifurcate from the steady solution we define the amplitude

$$\epsilon=\frac{1}{T}\int_0^T d\tau\, e^{-i\omega\tau}\mathbf{u}(\tau)\cdot\boldsymbol{\ell} , \tag{A4}$$

where $T=2\pi/\omega$ is the (unknown) period of oscillation of the sought periodic solution. Although μ is the physical control parameter, we discuss the problem in terms of ϵ: given a value of ϵ, at which value of μ can we find a periodic solution $\mathbf{u}(\tau)$ of Eq. (A1) that oscillates at a frequency ω and bifurcates from $\mathbf{u}=0$ at $\mu=\mu_{\mathrm{HB}}$? Hence we make the Taylor expansion

$$\mathbf{u}(\tau,\epsilon)=\epsilon\mathbf{u}_1(\tau)+\frac{1}{2!}\epsilon^2\mathbf{u}_2(\tau)+\cdots , \tag{A5a}$$

$$\omega(\epsilon)-\omega_0=\frac{1}{2!}\epsilon^2\omega_2+\frac{1}{4!}\epsilon^4\omega_4+\cdots , \tag{A5b}$$

$$\mu(\epsilon)-\mu_{\mathrm{HB}}=\frac{1}{2!}\epsilon^2\mu_2+\frac{1}{4!}\epsilon^4\mu_4+\cdots\ . \tag{A5c}$$

Note the absence of odd powers of ϵ in Eqs. (A5b) and (A5c). The even form of these expansions can be demonstrated [see after Eq. (VIII.35) of Ref. [25]]. Specifically, μ_2 controls whether the small-amplitude periodic orbit exists above ($\mu_2>0$, supercritical bifurcation) or below ($\mu_2<0$, subcritical bifurcation) the critical point $\mu=\mu_{\mathrm{HB}}$. The Floquet theory states that the periodic solution for small values of ϵ is stable when [cf. Eq. (VII.46) of Ref. [25]]

$$\epsilon\left[\frac{\partial\mu}{\partial\epsilon}\right]\left[\frac{\partial\alpha}{\partial\mu}\right]_{\mu=\mu_{\mathrm{HB}}}>0\ , \tag{A6}$$

where α is given in Eq. (A3c). For small values of ϵ, and according to Eq. (A5c), Eq. (A6) reads

$$\Sigma\equiv\mu_2\left[\frac{\partial\alpha}{\partial\mu}\right]_{\mu=\mu_{\mathrm{HB}}}>0\ , \tag{A7}$$

which indicates that the periodic solution will be stable if and only if it exists along the neighboring region of $\mu=\mu_{\mathrm{HB}}$, where the steady solution is unstable (exchange of stability). The computation of μ_2 is in general tedious and not straightforward. However, according to Eq. (VIII.35) of Ref. [25],

$$\Sigma=-\mathrm{Re}\left[\frac{1}{T}\int_0^T d\tau\, e^{-i\omega\tau}\ell\cdot[\mathbf{N}(\mu_{\mathrm{HB}};\mathbf{u}_1,\mathbf{u}_2)+\tfrac{1}{3}\mathbf{N}(\mu_{\mathrm{HB}};\mathbf{u}_1,\mathbf{u}_1,\mathbf{u}_1)]\right]\ . \tag{A8}$$

This way of writing Σ is more convenient since it involves quantities that are computed straightforwardly. Hence we must determine $\mathbf{u}_1(\tau)$ and $\mathbf{u}_2(\tau)$. Without loss of generality [cf. Eq. (VIII.30) of Ref. [25]]

$$\mathbf{u}_1(\tau)=e^{i\omega\tau}\kappa+e^{-i\omega\tau}\kappa^*\ . \tag{A9}$$

According to Eq. (VIII.27) of Ref. [25], which gives the evolution of $\mathbf{u}_2(\tau)$, we can write

$$\mathbf{u}_2(\tau)=\mathbf{u}_{2,2}e^{2i\omega\tau}+\mathbf{u}_{2,0}+\mathbf{u}_{2,-2}e^{-2i\omega\tau}\ , \tag{A10}$$

where the vectors $\mathbf{u}_{2,j}$ are constant. Inserting Eqs. (A9) and (A10) into Eq. (A8), the condition for stability of the periodic orbits reads

$$\mathrm{Re}\left\{\ell\cdot[\mathbf{N}(\mu_{\mathrm{HB}};\kappa,\mathbf{u}_{2,0})+\mathbf{N}(\mu_{\mathrm{HB}};\kappa^*,\mathbf{u}_{2,2})+\mathbf{N}_3(\mu_{\mathrm{HB}};\kappa,\kappa,\kappa^*)]\right\}<0\ , \tag{A11}$$

where the vectors $\mathbf{u}_{2,0}$ and $\mathbf{u}_{2,2}$ are given by

$$[\underline{L}(\mu_{\mathrm{HB}})-2i\omega_0]\mathbf{u}_{2,2}=-\mathbf{N}(\mu_{\mathrm{HB}};\kappa,\kappa)\ , \tag{A12a}$$

$$\underline{L}(\mu_{\mathrm{HB}})\mathbf{u}_{2,0}=-2\mathbf{N}(\mu_{\mathrm{HB}};\kappa,\kappa^*)\ . \tag{A12b}$$

Let us remark that Eq. (A12) complemented with Eqs. (A3) and (A13) are sufficient for the determination of the stability of the small-amplitude periodic solutions that emerge from the steady solution at a nondegenerate Hopf bifurcation *in any autonomous problem of the type (A1).* As κ and ℓ are norm-indetermined vectors it is essential to verify the normalization condition $\kappa\cdot\ell=1$.

Let us analyze now the stability of the periodic orbits arising at the Hopf bifurcation HBL affecting the steady solution $(0,E_2)$. We give only the main steps. In this case the matrix $\underline{L}$ has the form $\underline{L}=\underline{L}_2\otimes\underline{L}_1$, where $\underline{L}_2$ is the upper left-hand 4×4 submatrix in $\underline{L}$ [Eq. (11c)] and $\underline{L}_1$ the lower right-hand 3×3 submatrix. Since HBL is governed by $\underline{L}_2$, the right- and left-hand eigenvectors, κ and ℓ, are of the form

$$\kappa=(\kappa_1,\kappa_2,\kappa_3,\kappa_4,0,0,0)\ , \tag{A13a}$$

$$\ell=(\ell_1,\ell_2,\ell_3,0,0,0,0)\ . \tag{A13b}$$

It is worth noting that κ_i and ℓ_i $(i=1,2,3)$ are identical to the corresponding ones in the Lorenz-Haken model. Inserting Eq. (A14) into Eqs. (A12) and making use of the nonlinear vector $\mathbf{N}$ given in Eq. (A2) the condition for stability reads

$$(\kappa_1u_{20}^2+\kappa_2u_{20}^1+\kappa_1^*u_{22}^2+\kappa_2^*u_{22}^1)\ell_2-4(\kappa_2u_{20}^3+\kappa_3u_{20}^2+\kappa_2^*u_{22}^3+\kappa_3^*u_{22}^2)\ell_1<0\ , \tag{A14}$$

where u_{20}^i and u_{22}^j are the ith and jth components of vectors $\mathbf{u}_{2,0}$ and $\mathbf{u}_{2,2}$, respectively. Note that in Eq. (A14) only the first three components of κ, ℓ, $\mathbf{u}_{2,0}$, and $\mathbf{u}_{2,2}$ are present. Next we demonstrate that the first three components of $\mathbf{u}_{2,0}$ and $\mathbf{u}_{2,2}$ are identical to those corresponding to the Lorenz-Haken model.

From Eqs. (A12) the vectors $\mathbf{u}_{2,0}$ and $\mathbf{u}_{2,2}$ are given by

$$\mathbf{u}_{2,0}=-2[\underline{L}_2^{-1}\otimes\underline{L}_1^{-1}]\mathbf{N}(\mu_{\mathrm{HB}};\kappa,\kappa^*)\ , \tag{A15a}$$

$$\mathbf{u}_{2,2}=-[(\underline{L}_2-2i\omega_0)^{-1}\otimes(\underline{L}_1-2i\omega_0)^{-1}]\mathbf{N}(\mu_{\mathrm{HB}};\kappa,\kappa)\ . \tag{A15b}$$

It is simple to show that the fourth columns of both the submatrices $\underline{L}_2^{-1}$ and $(\underline{L}_2-2i\omega_0)^{-1}$ are of the form $(0,0,0,x)$. Thus according to (A16) the first three components of $\mathbf{u}_{2,0}$ and $\mathbf{u}_{2,2}$ are given by the first three components of the vectors $\mathbf{N}(\mu_{\mathrm{HB}};\kappa,\kappa^*)$ and $\mathbf{N}(\mu_{\mathrm{HB}};\kappa,\kappa)$, respectively. It is also simple to show that, according to Eq. (A2b) and Eq. (A13a), the first three components of the vectors $\mathbf{N}(\mu_{\mathrm{HB}};\kappa,\kappa)$ and $\mathbf{N}(\mu_{\mathrm{HB}};\kappa,\kappa^*)$ only contain the components κ_1, κ_2, and κ_3 that are identical to those of the Lorenz-Haken model. Hence we conclude that the Hopf bifurcation HBL has the same character of the Hopf bifurcation of the Lorenz-Haken model, that is, subcritical [20]. Hence the periodic orbit is unstable.

Concerning the Hopf bifurcation HBC, no clear analytical result is obtainable. Thus we have extensively tested the sign of Σ along a wide region of the parameter space. None of our calculations has given a negative Σ and hence we conclude that HBC is always supercritical, that is, the periodic orbit is stable.

[1] L. M. Narducci and N. B. Abraham, *Laser Physics and Laser Instabilities* (World Scientific, Singapore, 1988); N. B. Abraham, P. Mandel, and L. M. Narducci, in *Progress in Optics,* edited by E. Wolf (Elsevier, Amsterdam, 1988), Vol. XXIII, pp. 3–190; C. O. Weiss and R. Vilaseca, *Dynamics of Lasers* (VCH, Weinheim, 1991).

[2] H. Haken, R. der Agobian, and M. Pauthier, Phys. Rev. **140**, A437 (1965).

[3] O. Svelto, *Principles of Lasers* (Plenum, New York, 1989).

[4] (a) H. Schlemmer, D. Fröhlich, and H. Welling, Opt. Commun. **32**, 141 (1980); (b) J. Won, Opt. Lett. **8**, 79 (1983); J. Won and G. D. Willenberg, Appl. Phys. B **31**, 5 (1983).

[5] See A. W. Boone and S. Swain, Quantum Opt. **1**, 27 (1989), and references therein.

[6] G. J. de Valcárcel, E. Roldán, and R. Vilaseca, Phys. Rev. A **45**, R2674 (1992).

[7] D. J. Gauthier, Q. Wu, S. E. Morin, and T. W. Mossberg, Phys. Rev. Lett. **68**, 464 (1992).

[8] B. N. Nickolaus, D. Z. Zhang, and P. E. Toschek, Phys. Rev. Lett. **47**, 171 (1981).

[9] M. Brune, J. M. Raimond, P. Goy, L. Davidovich, and S. Haroche, Phys. Rev. Lett. **59**, 1899 (1987).

[10] Y. Zhu and X. S. Li, Phys. Rev. A **36**, 3889 (1987); Y. Zhu and M. O. Scully, *ibid.* **38**, 5433 (1988); A. W. Boone and S. Swain, *ibid.* **41**, 343 (1990).

[11] L. Davidovich, J. M. Raimond, M. Brune, and S. Haroche, in *Instabilities and Chaos in Quantum Optics II,* edited by N. B. Abraham, F. T. Arecchi, and L. Lugiato (Plenum, New York, 1988), p. 123.

[12] (a) C.-Z. Ning and H. Haken, Z. Phys. B **77**, 247 (1988); **77**, 157 (1989); (b) **77**, 163 (1989); (c) J. Zakrzewski and M. Lewenstein, Phys. Rev. A **45**, 2057 (1992).

[13] H. Haken, Phys. Lett. **53A**, 77 (1975).

[14] P. Mandel and O. Kocharovskaya, Phys. Rev. A **42**, 523 (1990); in *Nonlinear Dynamics and Quantum Phenomena in Optical Systems,* edited by R. Vilaseca and R. Corbalán, Springer Proceedings in Physics Vol. 55 (Springer, Berlin, 1992).

[15] O. Kocharovskaya and P. Mandel, Opt. Commun. **84**, 179 (1991).

[16] G. Bhanu Prasad and G. S. Agarwal, Opt. Commun. **86**, 409 (1991).

[17] L. M. Narducci, H. M. Doss, P. Ru, M. O. Scully, S. Y. Zhu, and C. Keitel, Opt. Commun. **81**, 379 (1991); **86**, 324 (1991); O. Kocharovskaya, F. Mauri, and E. Arimondo, *ibid.* **84**, 393 (1991); A. Karawajczyk, J. Zakrzewski, and W. Gawlik, Phys. Rev. A **45**, 420 (1992).

[18] J. Guckenheimer and P. Holmes, *Nonlinear Oscillations, Dynamical Systems and Bifurcations in Vector Fields* (Springer-Verlag, Berlin, 1983).

[19] E. Roldán, G. J. de Valcárcel, and R. Vilaseca, in *Nonlinear Dynamics and Quantum Phenomena in Optical Systems* (Ref. [14]), pp. 179–184.

[20] P. Mandel and H. Zeghlache, Opt. Commun. **47**, 146 (1983); H. Zeghlache, Ph.D. thesis, Université Libre de Bruxelles, 1988 (unpublished).

[21] S. Newhouse, D. Ruelle, and F. Takens, Commun. Math. Phys. **64**, 35 (1978).

[22] We have not analyzed whether the transition from quasiperiodic to chaotic motion occurs strictly through the Ruelle-Takens-Newhouse scenario [21] or its variant, the Curry-Yorke road to chaos [23].

[23] J. H. Curry and J. A. Yorke, in *The Structure of Attractors in Dynamical Systems,* edited by N. G. Markley, J. C. Martin, and W. Perrizo, Lecture Notes in Mathematics Vol. 668 (Springer-Verlag, Berlin, 1978), p. 48.

[24] H. Haken, *Advanced Synergetics* (Springer-Verlag, Berlin, 1984).

[25] G. Iooss and D. D. Joseph, *Elementary Stability and Bifurcation Theory* (Springer, New York, 1990).

[26] P. Mandel and T. Erneux, Opt. Acta **29**, 7 (1982).

[27] H. Zeghlache and V. Zehnlé, Phys. Rev. A **46**, 6015 (1992).